Correlation between Capacitance and Porosity in Microporous Carbon Monoliths.

A. Garcia-Gomez[1], V. Barranco[1], G. Moreno-Fernandez[1], J. Ibañez[2], T.A. Centeno[3] and J.M. Rojo[1]*

1. Instituto de Ciencia de Materiales de Madrid (ICMM), Consejo superior de Investigaciones Cientificas (CSIC); Sor Juana Ines de la Cruz, 3; Cantoblanco; E-28049 Madrid; Spain.

2. Centro Nacional de Investigaciones Matalurgicas (CENIM); CSIC; Av. Gregorio del Amo, 8; E-28040 Madrid; Spain.

3. Instituto Nacional del Carbon (INCAR); CSIC; Francisco Pintado Fe, 26; E-33080 Oviedo; Spain.

Corresponding author: jmrojo@icmm.csic.es

1

Abstract

Specific capacitance of carbons in aqueous KOH electrolyte seems to have two contributions, a double layer capacitance and a pseudo capacitance. Moreover, the specific capacitance increases as the specific surface area does. Here, we report that the pseudo capacitance is associated with the K^+ ion and the double layer capacitance with both K^+ and OH^- ion. The former ion dominates the capacitance of a real two-electrode supercapacitor. Two microporous carbon monoliths with surface areas similar for micropores below 0.63 nm but different for larger micropores are chosen. There is a correlation between the double layer capacitance due to those ions and the surface areas due to micropores with sizes above a certain value. It provides information on the size of those ions as they are electroadsorbed at the double layer. The dielectric permittivity associated with the K^+ and OH^- ion is discussed in relation to the confinement of these electroadsorbed ions in the micropores.

1. Introduction

Carbon monoliths consist of a three-dimensional network of carbon particles. They usually show a hierarchical porosity coming up from a suitable connectivity of macro/mesopores and micropores.[1-33] Carbon monoliths often show a high electrical conductivity, as a result of the good contact between adjacent particles.[16] Both hierarchical porosity and high electrical conductivity account for the application of carbon monoliths as supercapacitor electrodes.

Although carbon monoliths have been prepared for long time since the pioneer work by Saliger et al.[1], only in the last few years they have been studied as electrodes in their current form, i.e. as an entire piece of carbon.[8,13,15-22,26-30,32,33] Cells having carbon monoliths as electrodes have a number of advantages over those containing compacted pellets made from powder carbon. Previous works have shown that the cells with monolithic electrodes reach higher capacitance, lower resistance and shorter response time (i.e. faster charge/discharge).[16] Moreover, the three-dimensional character of the monolith has an effect on the electrical response of the cells.[17] As the monolith becomes thicker, (i) the cell capacitance increases significantly, (ii) the cell resistance is somewhat higher, and (iii) the response time becomes longer. Thus, thicker monoliths improve the cell energy whereas thinner monoliths lead to the enhancement of the cell power.[17,18] The main drawback of the carbon monoliths is their low density, typically below 0.5-0.6 g cm^{-3}.[1-5,17-32] Consequently, their volumetric capacitance does not surpass 100 F cm^{-3} in aqueous electrolytes and 50 F cm^{-3} in

organic ones. Recently, a volumetric capacitance as high as 342 F cm^{-3} has been reported for a carbon monolith combining high density and microporosity.[33]

The carbon monoliths can be prepared by different methods: (i) Carbonization of gels obtained from different carbon precursors and catalysts[1,5,7-12,20,21,28,29], (ii) Carbonization of gels involving a "template" that is removed either thermally, or chemically[3,19,24], (iii) Infiltration of inorganic monoliths with a carbon precursor, followed by carbonization of the precursor and removal of the inorganic template[3,4,10], (iv) Carbonization of a natural monolith, e.g. a piece of wood or bone[27,32], and (v) Mold conforming under pressure or by extrusion of a carbon precursor or powder carbon, followed by carbonization or activation.[15,17,22,26] A modification of the latter is the procedure patented by MAST Carbon Co to manufacture the cylindrical bars 650 CPI used in the present work. The bars were cut in smaller pieces also of cylindrical shape. They are the starting monoliths tested as electrodes. Some of the starting monoliths were additionally activated to modify the content of oxygen functionalities and the micropore size distribution while keeping the same specific surface area. They are the activated monoliths, also tested as electrodes.

The aim of the work is (i) to assess the contribution from pseudo capacitance and from double layer capacitance of the cations (K^+) and anions (OH^-) separately, (ii) to correlate the double layer capacitance of these ions with the surface area of micropores wider than a certain size, range 0.33-1.5 nm, in order to estimate the size of the two electroadsorbed ions, and (iii) to discuss the dielectric permittivity of the electroadsorbed ions in relation to their confinement in the micropores.

2. Experimental

Carbon bars of ca. 7 mm in diameter and 200 mm in length (reference 650 CPI) were produced through an extrusion method by MAST Carbon International Ltd. The bars were cut in slices of the same diameter and 2-3 mm in height. These items are the starting monoliths (SM) used as electrodes in this work. Some of them were activated under CO_2 flow (10 ml min^{-1}) at 800 ºC for 6 h, the weight loss (*burn-off*) being 7%. The activated monoliths are referred to as AM.

The monolith porosity was characterized by N_2 adsorption at 77 K (Micromeritics ASAP 2010) and by immersion calorimetry at 293 K (Tian Calvet-type calorimeter). The theoretical background is based on Dubinin´s theory and its extension to immersion calorimetry.[34, 35] The analysis of the N_2 adsorption isotherms by Dubinin-Radushkevich equation leads to the volume of the micropores, W_o, their average width, L_o, and the surface area of their walls, S_{mi}. Moreover, the comparison of the monolith isotherm with the data obtained for a non-porous carbon used as reference provides information on the total pore volume and the external (non microporous) surface area, S_e, of the monoliths.[35] In a first step, the total surface area of the monoliths was estimated from $S_{DR} = S_{mi} + S_e$.

In order to get a reliable determination of the specific surface area, the N_2 isotherm was also analyzed by other methods such as the comparison plot (S_{comp})[35] and the BET equation (S_{BET})[34]. These data were further cross-checked with the corresponding enthalpy of immersion of the carbon monoliths into dilute aqueous solution of phenol (S_{phenol}).[35]

The assessment of the micropore accessibility was got from the enthalpies of immersion (Δ_iH) into liquids having critical molecular sizes between 0.33 and 1.5 nm. Therefore, the micropore size distribution was derived by using probes such as dichloromethane (0.33 nm), benzene (0.41 nm), carbon tetrachloride (0.63 nm), cyclododeca-1,5,9-triene CDDT (0.76 nm) and tri-2,4-xylylphosphate TXP (1.50 nm). This technique has been described in detail elsewhere. [34]

Temperature-programmed desorption (TPD) experiments were carried out to characterize the surface chemistry of the two types of monoliths. The measurements were performed in a TGA (SDT Q600, TA Instruments) which was coupled to a quadrupole mass spectrometer (Thermostar GSD 300 T3, Balzers Instruments). The monoliths were ground in agate mortar and approximately 15 mg of the powder samples were heated at a rate of 10 ºC min^{-1} up to 950 ºC, keeping this temperature for 30 minutes. The experiments were carried out under a helium flow of 100 ml min^{-1}. For quantifying the CO and CO_2 evolved, the intensities of the CO and CO_2 signal were measured. Calcium oxalate was used as reference material.

The microstructure of the monoliths was analyzed by Scanning Electron Microscopy (SEM). Images were obtained in the secondary electron mode by a Hitachi S-4800. Quantitative image analysis was carried out on polished monoliths, which were previously embedded in a resin.

Electrical conductivity measurements were carried out in a two-probe system at room temperature. The two circular areas of the carbon monoliths were painted with a commercial silver paint, and then heated at 80 ºC overnight. The monolith

resistance was measured on monoliths of several heights according to the fact that the monolith resistance must be higher than the system resistance, at least 5-10 times higher.

The electrochemical study was performed in a three-electrode cell. The carbon monoliths, either SM or AM, acted as working electrodes. Hg/HgO was the reference electrode. A Pt wire coiled on the reference electrode was the counter electrode. The electrolyte was 1M KOH aqueous solution. Cyclic voltammetries were performed at a voltage scan rate of 0.1 mV s^{-1}. Galvanostatic measurements were carried out at 1 mA cm^{-2} (or 4.2 mA g^{-1}). For comparison, galvanostatic measurements in two-electrode cells were carried out at that current density. Before the electrochemical measurements, the carbon monoliths were immersed into the KOH solution under primary vacuum (ca. 10^{-1} Torr) for 1 h. This treatment favored the removal of adsorbed air as bubbles and the access of the electrolyte to the monolith carbon particles. Then, the electrolyte was kept in contact with the monoliths for 1 day. To check the hydrophilic character of the monoliths against the KOH solution, the contact angles between the surface of drops of that solution and a flat surface of the carbon monoliths were measured. To get a flat surface, the carbon monoliths were previously polished.

3. Results and discussion

3.1 Microstructural, textural and chemical characterization

A top view of the starting monolith (SM) is shown in Figure 1a. This monolith, of 7.2 mm in diameter, shows carbon walls (black) and channels (grey) both addressed

along the cylinder axis. The presence of channels favors the access of the electrolyte to the carbon walls. However, the presence of these channels leads to a low density of SM, 0.66 g cm^{-3}. The thickness of the carbon walls is 0.43 mm. The edge of the squared channels is 0.62 mm. The geometrical surface area of the carbon at the circular base is 0.33 cm^2; this is the area taken to calculate the current density. The monolith height is 3 mm and the monolith weight is 78 mg. The SEM image of the same monolith
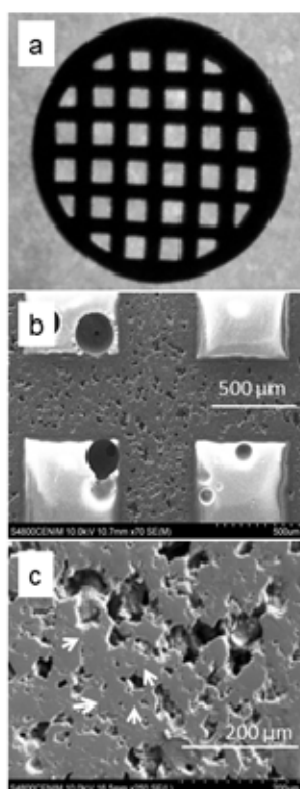

Figure 1. Top view picture of the starting carbon monolith (7.2 mm in diameter) showing the carbon walls in black and the channels in grey (a). SEM pictures of the carbon walls at low (b) and high (c) magnification.

embedded in a resin and then polished is shown in Figure 1b. The carbon walls show some voids of micrometer size, ca. 10-20 μm, and non-uniform shape. The presence of these voids can favor the access of the electrolyte to the interior of the carbon walls. An additional magnification illustrates that the carbon walls are made of well-

8

connected carbon particles, i.e. without borders between adjacent particles (see arrows in Figure 1c). The size of the carbon particles is ca. 20-50 μm. The good contact between adjacent particles agrees with the high electrical conductivity found for SM, 6.5 S cm^{-1}. The microstructure of the activated monolith (AM) (not shown) is similar to that of SM. In accordance with it, the density and electrical conductivity of SM and AM are rather close (Table 1).

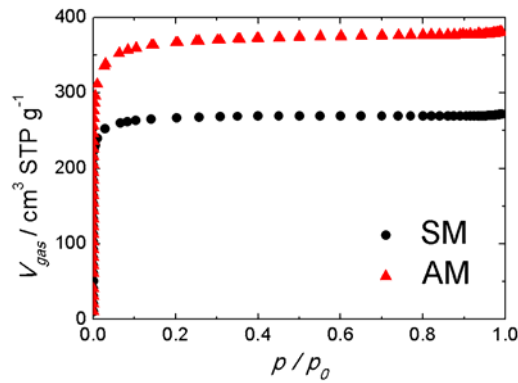The type I-shape observed for the nitrogen adsorption isotherms (Figure 2)

Figure 2. Nitrogen adsorption isotherms of the starting (SM) and the activated (AM) carbon monolith.

Table 1. Textural, physical and chemical characteristics of the starting (SM) and activated (AM) carbon monolith.

	SM	AM
W_0 (cm^3 g^{-1})	0.42	0.58
L_0 (nm)	0.73	1.01
S_{mi} (m^2 g^{-1})	1151	1148
S_e (m^2 g^{-1})	1	3
$S_{DR} = S_{mi} + S_e$ (m^2 g^{-1})	1152	1151
S_{comp} (m^2 g^{-1})	1107	1057
S_{phenol} (m^2 g^{-1})	1000	1193
S_{BET} (m^2 g^{-1})	619	1039
S_{total} [a] (m^2 g^{-1})	1086	1134

$-\Delta_i H[CH_2Cl_2\ 0.33nm]$ (J g^{-1})	142.7	193.2
$-\Delta i H[C_6H_6\ 0.41\ nm]$ (J g^{-1})	146.6	192.5
$-\Delta_i H[CCl_4\ 0.63\ nm]$ (J g^{-1})	128.2	181
$-\Delta_i H[CDDT^{(b)}\ 0.76nm]$ (J g^{-1})	47.1	154
$-\Delta_i H[TXP^{(c)}\ 1.50\ nm]$ (J g^{-1})	2.0	6.27
Density (g cm^{-3})	0.66	0.61
Conductivity (S cm^{-1})	6.5	6
[CO] (μmol g^{-1})	933	913
[CO$_2$] (μmol g^{-1})	457	166

[a] $S_{total} = (S_{comp} + S_{phenol} + S_{DR})/3$

[b] CDDT is cyclododeca-1,5,9-triene

[c] TXP is tri-2,4-xylylphosphate

indicates that both monoliths are essentially microporous. As reported in Table 1, where the main porous characteristics are summarized, the SM shows a microporous surface area, S_{mi} =1151 m^{2}g^{-1} and an average micropore size, L_o=0.73 nm. The contribution from pores wider than 2 nm is negligible as indicated by the external surface area, S_e =1 m^{2}g^{-1}. The activation process leads to a significant increase in the micropore volume (W_o = 0.58 cm^3 g^{-1}) as well as the widening of the micropores (L_o=1.01 nm). However, the S_{mi} and S_e are not significantly modified. The AM displays a total surface area, S_{DR}, similar to that of the SM.

Based on immersion calorimetry, the profile of the micropore volume accessible to molecules with critical dimensions between 0.33 and 1.5 nm, confirms a narrow micropore size distribution, with the majority of the micropores in the range 0.63-0.76 nm for SM (Figure 3a) and in the range 0.76-1.5 nm for AM (Figure 3b). The

good agreement between both adsorption and immersion experiments indicates the absence of "gate" effects at the entrance of the micropores.
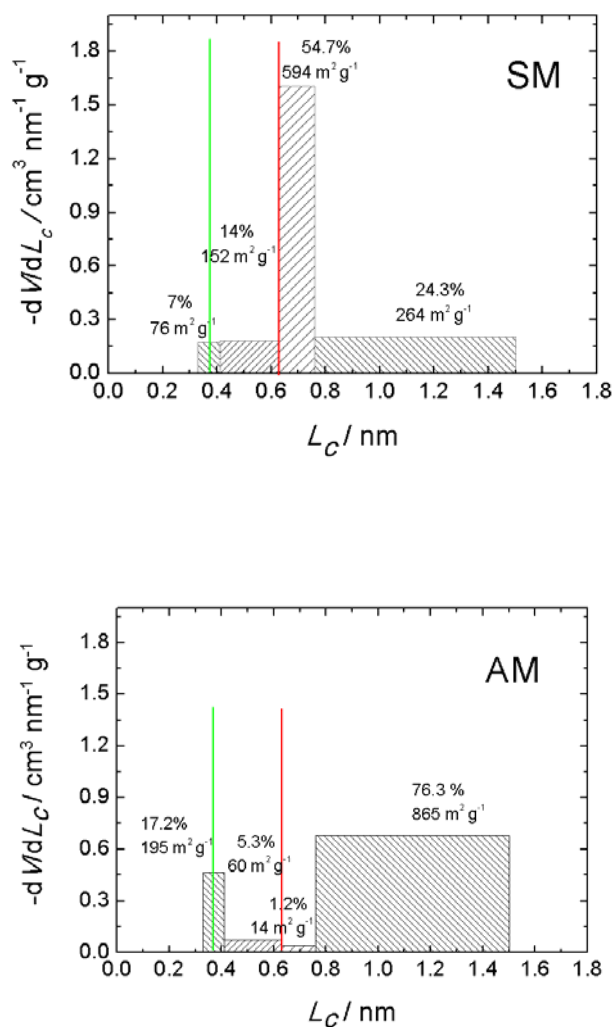

Figure 3. Micropore size distributions obtained for the carbon monoliths SM (top) and AM (bottom). The surface areas, expressed in m^2g^{-1} and percentage, associated with each micropore range is shown. Green and red lines indicate the minimum micropore size available for electroadsorption of K^+ ions (0.37 nm) and OH^- ions (0.63 nm).

As reported in Table 1, the Dubinin-Raduskevich approach (S_{DR}), the comparison plot (S_{comp}) and the immersion calorimetry into aqueous solution of phenol (S_{phenol}), lead to similar values for the specific surface area. In agreement with that

previously reported,[35,36] the surface area estimated by the BET equation (S_{BET}) differs from the other surface areas for SM; it is due to a high contribution of the micropores smaller than 0.9 nm to the surface area. In contrast, S_{BET} agrees with the other determinations for AM with an average micropore size of 1 nm. Based on these results, one may take the average value, $S_{total} =(S_{comp} + S_{phenol} + S_{DR})/3$, as the best estimation for the total surface area of the two carbon monoliths, S_{total} being 1086 $m^2 g^{-1}$ for SM and 1134 $m^2 g^{-1}$ for AM.

Taking into account the values of S_{total} and the pore size distributions found for the two monoliths, the surface areas associated with the micropores in the ranges of 0.33-0.41 nm, 0.41-0.63 nm, 0.63-076 nm and 0.76-1.5 nm have been estimated (see Figures 3a and 3b). Comparing the two monoliths, most of the surface area is due to micropores in the range 0.63-0.76 nm for the SM and in the range 0.76-1.5 nm for the AM. These differences will be discussed in relation to the capacitances of the K^+ and OH^- ions below. Regarding the surface chemistry, the activation does not affect the content of oxygen functionalities desorbing as CO in TPD experiments but notably decreases the surface groups desorbing as CO_2 (Table 1).

3.2 Electrochemical study

The hydrophilic character of the two monoliths against the KOH solution is confirmed by the low contact angle measured, 22-30 º. This contact angle is the angle appearing between the surface of solution drops and the flat surface of the carbon monoliths. The effect of the concentration of KOH solution on the capacitance of activated carbon and carbon cloth has been reported elsewhere.[37, 38] In this work, the

1M concentration was chosen because the pseudo capacitance of carbon electrodes has been reported for this concentration as discussed below. Moreover, the 1M concentration is the usually reported in literature.

The galvanostatic plots obtained for SM in two- and three-electrode cell are shown as examples in Figures 4a and 4b, respectively. In both cases, the measurements were carried out at 1 mA cm^{-2} (or 4.2 mA g^{-1}). This low current density was chosen to monitor the capacitance under steady conditions, i.e. the capacitance measured is only due to the carbon monolith and is not affected by any kinetic effect. In the two-electrode configuration, the specific capacitance was determined according to C 2E= 2·I·t_d/E_2·m, where I is the current applied, t_d is the discharge time, E_2 is the voltage decrease during discharge and m is the mass of one monolith (Figure 4a). The C 2E values found are 138 and 143 F g^{-1} for SM and AM, respectively, i.e. nearly the same specific capacitance.
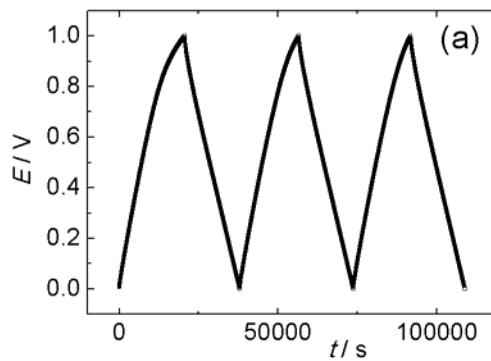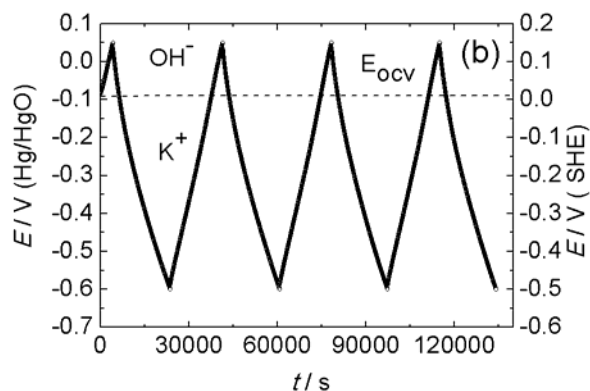
Figure 4. Galvanostatic charge/discharge plots recorded at 1 mA cm^{-2} for the SM carbon monolith in two-electrode (a) and three-electrode (b) cell.

Further information is obtained from the three-electrode cell (Figure 4 b). In the voltage range from the open circuit voltage (E$_{OCV}$) to positive voltages, the electroadsorption/ electrodesorption of the OH$^-$ ions happens. This includes the formation of the double layer as well as possible reversible redox reactions of the OH$^-$ ions with functional groups of the carbon surface (pseudo capacitance contribution). The same applies for the K$^+$ ions in the voltage range from E$_{OCV}$ to negative voltages. During the discharge over the complete voltage range, i.e. from 0.05 to -0.6 V, the specific capacitance is due to the contribution of the two ions and is determined according to C 3E= $I \cdot t_d / E_2 \cdot m$, where m is the mass of the monolith and the other parameters have the same meanings as discussed for the two-electrode cell. The C 3E obtained is 145 and 146 F g^{-1} for SM and AM, respectively. Within the experimental error, C 2E and C 3E are nearly the same despite the different voltage ranges, ca. 1 V for the two-electrode cell, and ca. 0.7 V for the three-electrode configuration.

14

The specific capacitance due to the OH⁻ (C_{OH^-}) was obtained from the galvanostatic plots in the range E_{OCV} - positive voltages (Figure 5a). That due to the K⁺ (C_{K^+}) was determined from galvanostatic plots in the range E_{OCV} - negative voltages (Figure 5b). The upper voltage for OH⁻ is limited to ca. 0.06 V. Above this voltage,
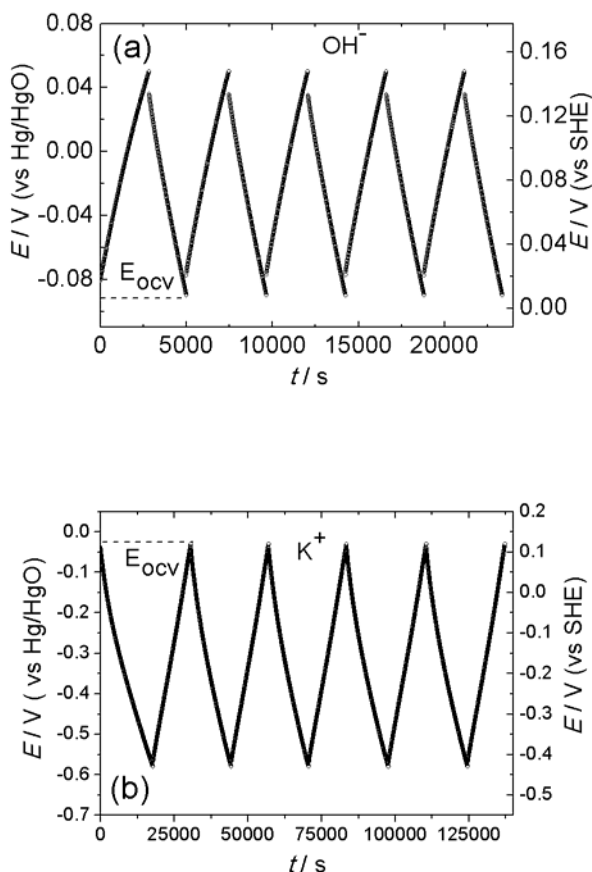
Figure 5. Galvanostatic charge/discharge plots recorded at 1mA cm⁻² for the SM carbon monolith in three-electrode cell. The electrochemical response due to the OH⁻ and K⁺ ion is shown in (a) and (b), respectively.

oxygen evolution due to water decomposition happens. Then, the voltage window for OH⁻ is as narrow as 0.15 V. In contrast, the lowest voltage for K⁺ is -0.6 V, and even more because hydrogen evolution is observed for voltages close to -1 V *vs.* Hg/HgO.

Then, the voltage window for the K$^+$ (ΔV_{K+}), around 1 V, is much broader than that for the OH$^-$ (ΔV_{OH-}). The former contributes more to the total voltage range, $\Delta V = \Delta V_{K+} + \Delta V_{OH-}$, in a real supercapacitor. The values obtained for C_{K+} and C_{OH-} together with those obtained for C 2E and C 3E are summarized in Table 2. For the two monoliths, C_{K+} is higher than C_{OH-}, which agrees with that reported for other powder

Table 2. Specific capacitance due to K$^+$ (C_K^+) and OH$^-$ (C_{OH}^-) and the corresponding contributions from the pseudocapacitance (C (PS)) and the double layer capacitance (C (DL)). The values of specific capacitance obtained in two-electrode (C 2E) and three-electrode (C 3E) cell are also reported.

Monolith	C_K^+ F g^{-1}	C_K^+(PS) F g^{-1}	C_K^+(DL) F g^{-1}	C_{OH}^- F g^{-1}	C_{OH}^- (DL) F g^{-1}	C 2E F g^{-1}	C 3E F g^{-1}
SM	128	33	95	82	82	138	145
AM	137	32	105	84	84	143	146

microporous carbons.[39] Moreover, the values of C_{K+} are close to those of C 2E and C 3E, i.e. to the capacitances in which both ions are involved. It points out the higher contribution from K$^+$ ions to the capacitance measured in a real supercapacitor. These ions, which show higher specific capacitance and broader voltage window, dominate the electrochemical response of the two monoliths, SM and AM. The contribution of each ion to the capacitance of a real supercapacitor, i.e. a two-electrode supercapacitor, can be estimated according to the equation:

$$C = (C_{K+} \cdot \Delta V_{K+} + C_{OH-} \cdot \Delta V_{OH-}) / (\Delta V_{K+} + \Delta V_{OH-}) \quad (1)$$

Taking as an example the values of C_{K+} and C_{OH-} from Table 2 on the one hand, and the values of $\Delta V_{OH-}=0.15$ V and $\Delta V_{K+}=0.85$ V for a total voltage window of 1 V on the other,

the contribution of the K^+ ions to C is 90 % for both monoliths, SM and AM. Moreover, it is worth to note that eq. (1) differs from the equation

$$1/C = 1/C_{K+} + 1/C_{OH-} \quad \text{or} \quad C = C_{K+} \cdot C_{OH-}/(C_{K+} + C_{OH-}) \tag{2}$$

some times proposed to calculate the specific capacitance in a two-electrode cell from the specific capacitances of the K^+ and OH^- ion determined in a three-electrode cell.

To assess whether C_{K+} and C_{OH-} are affected by a pseudo capacitance in addition to the double layer capacitance, the cyclovoltammetries associated with the K^+ and OH^- ion were recorded separately (Figure 6). The rectangular shape characteristic of
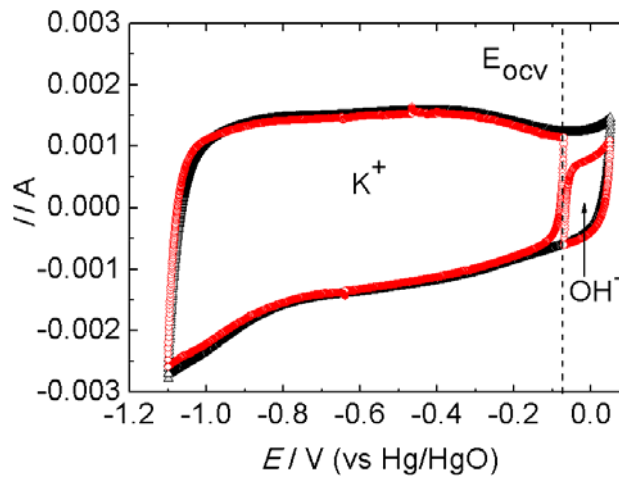

Figure 6. Cyclic voltammetries recorded in three-electrode cell for the SM carbon monolith. The electrochemical response of K^+ and OH^- ion (red circles) and the total voltammetry (black triangles) are shown. The measurements were carried out at the voltage scan rate of 0.1 mV s^{-1}.

the double layer is observed for the OH^- ions; it indicates that C_{OH-} is essentially a double layer capacitance, $C_{OH-}(DL)$, and hence $C_{OH-} = C_{OH-}(DL)$. In contrast, the presence of some humps at ca. -0.3 and -0.9 V for the K^+ ions provides evidence of a pseudo capacitance, $C_{K+}(PS)$, in addition to the double layer capacitance, $C_{K+}(DL)$; hence, $C_{K+} =$

17

C_{K+}(PS) + C_{K+}(DL). A pseudo capacitance associated with the K^+ ions has been reported for MnO_2 since the pioneer works by Goodenough et al.[40] and by Anderson et al.[41] In carbons having different oxygen groups, e.g. ketone, carboxylic acid, anhydrides, etc., the presence of a pseudocapacitance has also been found.[38,42-49] The pseudocapacitive contribution in the aqueous electrolytes sulfuric acid and potassium hydroxide has been estimated from the linear dependences found on the CO-generating oxygen groups, the latter as determined from TPD measurements.[47,49] For microporous carbons in the 1M KOH aqueous solution, the pseudocapacitance was found to be 0.035±0.005 F µmol^{-1} of CO.[49] Then, for our carbon monoliths C_{K+}(PS) can be estimated according to:

$$C_{K+}(PS)=(0.035 \text{ F µmol}^{-1} \text{ of CO})\times(CO \; content) \tag{3}$$

where the CO *content* is expressed in µmol of CO per gram of sample. The values of C_{K+}(PS) for the two monoliths are close (Table 2) in agreement with their similar contents of CO (Table 1). Then, the values of C_{K+}(DL) can be calculated by subtraction of C_{K+}(PS) from C_{K+}. For the two monoliths, the contributions of C_{K+}(PS) and C_{K+}(DL) are ca. 25% and 75%, respectively. Moreover, the values of C_{K+}(DL) are higher (ca. 1.2 times) than those of C_{OH-}(DL) (Table 2).

Assuming that the double layer capacitance of each ion must be proportional to the surface area accessible to the ion, the comparison of the ratio C_{K+}(DL)/C_{OH-}(DL) with the ratio of the surface areas due to micropores larger than 0.33, 0.41, 0.63 and 0.76 nm (respectively, $S_{0.33}$, $S_{0.41}$, $S_{0.63}$ and $S_{0.76}$) can provide information on the size of the electroadsorbed K^+ and OH^- ions at the double layer. As shown in Table 3 for the monolith AM, the ratio C_{K+}(DL)/C_{OH-}(DL) is close to the ratios $S_{0.33}$/ $S_{0.63}$, $S_{0.41}$/$S_{0.63}$, $S_{0.33}$/

$S_{0.76}$ and $S_{0.63}/S_{0.76}$. Then, there are more than one possibility for the size of electroadsorbed K^+ and OH^-: either 0.33 and 041 nm for K^+ and 0.63 nm for OH^- or 0.63 nm for K^+ and 0.76 nm for OH^-. The pore size distribution of AM does not permit to elucidate on the size of the two electroadsorbed ions. However, for the monolith SM, the ratio $C_{K+}(DL)/C_{OH-}(DL)$ is close to the ratios $S_{0.33}/S_{0.63}$ and $S_{0.41}/S_{0.63}$ but differs from the ratios $S_{0.33}/S_{0.76}$ and $S_{0.63}/S_{0.76}$, the two latter clearly surpassing the capacitance

Table 3. Comparison of the ratio of the double layer capacitances due to K^+ and OH^- with the ratio of the surface areas due to micropores wider than 0.33, 0.41, 0.63 and 0.76 nm.

Monolith	$C_{K+}(DL)/C_{OH-}(DL)$	$S_{0.33}/S_{0.63}$	$S_{0.41}/S_{0.63}$	$S_{0.33}/S_{0.76}$	$S_{0.63}/S_{0.76}$
SM	1.16	1.26	1.18	4.11	3.25
AM	1.25	1.29	1.07	1.31	1.02

ratio. These results point out that the electroadsorbed K^+ ions have a size compatible with micropores wider than 0.33-0.41 nm and the electroadsorbed OH^- ions with micropores larger than 0.63 nm. Then, a size of around 0.37 nm (average value of 0.33 and 0.41 nm) and a size of 0.63 nm can be ascribed to the electroadsorbed K^+ and OH^-, respectively. The value obtained for K^+ fits within the range 0.36-0.42 nm proposed from a systematic study of powder carbons having narrow micropore size distributions, and hence acting as sieves.[50,51] The size of 0.37 nm for electroadsorbed K^+ agrees with the size of K^+ ions hydrated with three water molecules (0.41 nm).[52] That value clearly differs from the size of 0.77 nm estimated for K^+ hydrated with six water molecules.[53] Regarding the size of 0.63 nm for electroadsorbed OH^-, it agrees with that of OH^- ions hydrated with three water molecules (0.60 nm) but differs from the size of dehydrated

OH$^-$ (0.26 nm).[54,55] The present results indicate that both K$^+$ and OH$^-$ are hydrated when electroadsorbed on the microporous carbon surface.

The double layer capacitance associated with the cation and the anion and normalized by the available surface area, i.e. by the surface area due to micropores wider than 0.37 nm for K$^+$ and wider than 0.63 nm for OH$^-$, is outlined in Table 4. A

Table 4. Double layer capacitance due to K$^+$ and OH$^-$ normalized by the surface areas of micropores with sizes compatible with the dimensions of the electroadsorbed ions. For comparison, the values normalized by the total surface areas are also shown.

Monolith	$C_{K+}(DL)/S_{0.37}$ F m^{-2}	$C_{K+}(DL)/S_{total}$ F m^{-2}	$C_{OH^-}(DL)/S_{0.63}$ F m^{-2}	$C_{OH^-}(DL)/S_{total}$ F m^{-2}
SM	0.091	0.087	0.096	0.075
AM	0.101	0.093	0.096	0.074

contribution similar from both ions of around 0.096 Fm^{-2} is found. In contrast, as the total surface areas estimated by N$_2$ adsorption (S$_{total}$) are considered, the normalized double layer capacitances shift towards lower values, ca. 0.90 F m^{-2} for K$^+$ and ca. 0.075 F m^{-2} for OH$^-$. It stresses that areas taking into account the size of the electroadsorbed ions lead to more reliable results.

The dielectric permittivity due to those ions has been estimated on the basis of the sandwich model for slit-shaped micropores.[56] The hypothesis of this shape is supported by the agreement between S_{phenol}, S_{comp} and S_{DR}, the latter assuming slits for micropores (Table 1). According to the sandwich model:

$$C/S = \varepsilon_r \varepsilon_0/(b-a_0) \qquad\qquad (3)$$

where C is the double layer capacitance, either $C_{K^+}(DL)$ or $C_{OH^-}(DL)$. S is the surface area accessible to the ions, i.e. $S_{0.37}$ for K$^+$ and $S_{0.63}$ for OH$^-$. ε_r is the relative dielectric permittivity for each ion. ε_0 is the dielectric permittivity in vacuum. $2b$ is the micropore width and $2a_0$ is the ion diameter. Taking the ion size ($2a_0$) as 0.37 nm for the electroadsorbed K$^+$ and 0.63 nm for electroadsorbed OH$^-$ ions, the values of ε_r have been estimated for the two ions in the two monoliths (SM and AM). Figure 7 shows the dependence of ε_r as a function of $2b$. Owing to C/S shows nearly the same value for
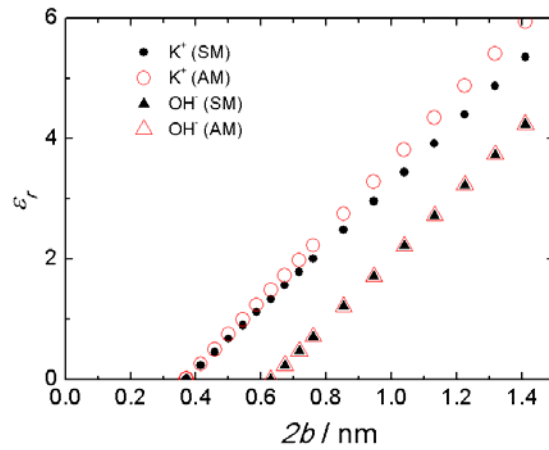

Figure 7. Dependence of the dielectric permittivity as a function of the micropore size for the K$^+$ ions (circles) and OH$^-$ ions (triangles). Closed and open symbols stand for the carbon monoliths SM and AM, respectively.

the two monoliths, the corresponding ε_r values are close. For a given micropore size, however, the value of ε_r is higher for K$^+$ than for OH$^-$. It is associated with the smaller size of the electroadorbed K$^+$ as compared to the electroadsorbed OH$^-$. For the two types of ions, ε_r increases as the micropore size does; it means that ε_r increases as the electroadsorbed ion is less confined in the micropores. The change in the confinement seems to be associated with a change in the site of the K$^+$ ions and also in the number

21

of water molecules within the micropores, as deduced from molecular dynamic simulations.[56]

4. Conclusions

The two carbon monoliths studied in this work show a high electrical conductivity (6-6.5 S cm^{-1}) but a moderate density (0.61-0.66 g cm^{-3}). The former as a consequence of the good contact between adjacent carbon particles, the latter due to the presence of channels. The monoliths show a porosity coming from micropores with sizes in the range 0.33-1.5 nm; their pore size distribution is similar for sizes below 0.63 nm but different for larger micropores. The two monoliths display large and similar specific surface areas, ca. 1000 m^2 g^{-1}.

The specific capacitance due to the K$^+$ ions is about 60 % higher than that due to the OH$^-$ ions. This comes from a pseudo capacitive contribution, ca. 25 % from total capacitance, to be added to the double layer capacitance. The OH$^-$ ions show exclusively the double layer capacitance. The higher specific capacitance and broader voltage window of the K$^+$ ions compared to the OH$^-$ ones, account for a much higher contribution of the cations (90 %) for storing energy in a real two-electrode supercapacitor.

For the two monoliths, the double layer capacitance of the cations is higher (1.2 times) than that of the anions as a consequence of the smaller size of the electroadsorbed K$^+$ ($\approx$ 0.37 nm) compared to the electroadsorbed OH$^-$ (0.63 nm). Both ions are electroadsorbed in their hydrated state.

Based on the sandwich model the dielectric permittivity of the two ions increases as the micropore width increases, i.e. as the electroadsorbed ion is less confined in the micropore. For the same micropore size, the dielectric permittivity is higher for K^+ than for OH^- because the electroadsorbed cation is smaller.

References

(1) Saliger, R.; Fischer, U.; Herta, C.; Fricke, J. High Surface Area Carbon Aerogels for Supercapacitors. *J. Non-Cryst. Solids* **1998**, 225, 81-85.

(2) Yang, H.; Shi, Q.; Liu, X.; Xie, S.; Jiang, D.; Zhang, F.; Yu, C.; Tu, B.; Zhao, D. Synthesis of Ordered Mesoporous Carbon Monoliths with Bicontinuous Cubic Pore Structure of Ia3d Symmetry. *Chem. Commun.* **2002**, 2842-2843.

(3) Yu, J.-S.; Kang, S.; Yoon, S.B.; Chai, G. Fabrication of Ordered Uniform Porous Carbon Networks and Their Application to a Catalyst Supporter. *J. Am. Chem. Soc.* **2002**, 124, 9382-9383.

(4) Taguchi, A.; Smatt, J.H.; Linden, M. Carbon Monoliths Possessing a Hierarchical, Fully Interconnected Porosity. *Adv. Mater.* **2003**, 15, 1209-1211.

(5) Wu, D.; Fu, R.; Zhang, S.; Dresselhaus, M.S.; Dresselhaus, G. Preparation of Low-Density Carbon Aerogels by Ambient Pressure Drying. *Carbon* **2004**, 42, 2033-2039.

(6) Baumann, T.F.; SatcherJr, J.H. Template-Directed Synthesis of Periodic Macroporous Organic and Carbon Aerogels. *J. Non-Cryst. Solids* **2004**, 350, 120-125.

(7) Tonanon, N.; Siyasukh, A.; Wareenin, Y.; Charinpanitkul, T.; Nishihara, H.; Mukai, S.R.; Tamon, H. 3D Interconnected Macroporous Carbon Monoliths Prepared by Ultrasonic Irradiation. *Carbon* **2005**, 43, 2808-2811.

(8) Kim, S.J.; Hwang, S.W.; Hyun, S.H. Preparation of Carbon Aerogel Electrodes for Supercapacitors and Their Electrochemical Characteristics. *J. Mater. Sci.* **2005**, 40, 725-731.

(9) Mukai, S.R.; Nishihara, H.; Yoshida, T.; Taniguchi, K.; Tamon, H. Morphology of Resorcinol-Formaldehyde Gels Obtained Through Ice-Templating. *Carbon* **2005**, 43, 1563-1565.

(10) Zhou, Z.; Yan, Q.; Su, F.; Zhao, X.S. Replicating Novel Carbon Nanostructures with 3D Macroporous Silica Template. *J. Mater. Chem.* **2005**, 15, 2569-2574.

(11) Liu, N.; Zhang, S.; Fu, R.; Dresselhaus, M.S.; Dresselhaus, G. Fabrication and Structure of Carbon Aerogel Spheres Prepared by Inverse Suspension/Emulsion Polymerization and Ambient Pressure Drying. *J. Appl. Polymer Sci.* **2007**, 104, 2849-2855.

(12) Li, J.; Wang, X.; Wang, Y.; Huang, Q.; Dai, C.; Gamboa, S.; Sebastian, P.J. Structure and Electrochemical Properties of Carbon Aerogels Synthesized at Ambient Temperature as Supercapacitors. *J. Non-Cryst. Solids* **2008**, 354, 19-24.

(13) Batalla Garcia, B.; Feaver, A.M.; Zhang, Q.; Champion, R.D.; Cao, G.; Fister, T.T.; Nagle, K.P.; Seidler, G.T. Effect of Pore Morphology on the Electrochemical Properties of Electric Double Layer Carbon Cryogel Supercapacitors. *J. App. Phys.* **2008**, 104, 014305 (1-9).

(14) Xu, S.; Li, J.; Qiao, G.; Wang, H.; Lu, T. Pore Structure Control of Mesoporous Carbon Monoliths Derived from Mixtures of Phenolic Resin and Ethylene Glycol. *Carbon* **2009**, 47, 2103-2111.

(15) Ruiz, V.; Blanco, C.; Santamaria, R.; Ramos-Fernandez, J.M.; Martinez-Escandell, M.; Sepulveda-Escribano, A.; Rodriguez-Reinoso, F. An Activated Carbon Monolith as an Electrode Material for Supercapacitors. *Carbon* **2009**, 47, 195-200.

(16) Garcia-Gomez, A.; Miles, P.; Centeno, T.A.; Rojo, J.M. Why Carbon Monoliths Are Better Supercapacitor Electrodes Than Compacted Pellets. *Electrochem. Solid-State Lett.* **2010**, 13(8), A112-A114.

(17) Garcia-Gomez, A.; Miles, P.; Centeno, T.A.; Rojo, J.M. Uniaxially Oriented Carbon Monoliths as Supercapacitor Electrodes. *Electrochim. Acta* **2010**, 55, 8539-8544.

(18) Chmiola, J.; Largeot, C.; Taberna, P.L.; Simon, P.; Gogotsi, Y. Monolithic Carbide-Derived Carbon Films for Micro-Supercapacitors. *Science* **2010**, 328, 480-483.

(19) Bruno, M.M.; Cotella, N.G.; Miras, M.C.; Barbero, C.A. A Novel Way to Maintain Resorcinol-Formaldehyde Porosity During Drying: Stabilization of the Sol-Gel Nanostructure Using a Cationic Polyelectrolyte. *Colloids Surfaces A: Physicochem. Eng. Aspects* **2010**, 362, 28-32.

(20) Carriazo, D.; Pico, F.; Gutierrez, M.C.; Rubio, F.; Rojo, J.M.; del Monte, F. Block-Copolymer Assisted Synthesis of Hierarchical Carbon Monoliths Suitable as Supercapacitor Electrodes. *J. Mater. Chem.* **2010**, 20, 773-780.

(21) Halama, A.; Szubzda, B.; Pasciak, G. Carbon Aerogels as Electrode Materials for Electrical Double Layer Supercapacitors. Synthesis and Properties. *Electrochim. Acta* **2010**, 55, 7501-7505.

(22) Taer, E.; Deraman, M.; Talib, I.A.; Awitdrus, A.; Hashmi, S.A.; Umar, A.A. Preparation of a Highly Porous Binderless Activated Carbon Monolith from Rubber Sawdust by a Multi-Step Activation Process for Application in Supercapacitors. *Int. J. Electrochem. Sci.* **2011**, 6, 3301-3315.

(23) Biener, J.; Stadermann, M.; Suss, M.; Worsley, M. A.; Biener, M.M.; Rose, K.A.; Baumann, T.F. Advanced Carbon Aerogels for Energy Applications. *Energy Environ. Sci.* **2011**, 4, 656-667.

(24) Brun, N.; Prabaharan, S.R.S.; Surcin, C.; Morcrette, M.; Deleuze, H.; M. Birot, M.; Babot, O.; Achard, M.F.; Backov, R. Design of Hierarchical Porous Carbonaceous Foams from a Dual-Template Approach and Their Use as Electrochemical Capacitor and Li Ion Battery Negative Electrodes. *J. Phys. Chem. C* **2012**, 116, 1408-1421.

(25) Candelaria, S.L.; Chen, R.; Jeong, Y.-H.; Cao, G. Highly Porous Chemically Modified Carbon Cryogels and Their Coherent Nanocomposites for Energy Applications. *Energy Environ. Sci.*, **2012**, 5, 5619-5637.

(26) Awitdrus, A.; Deraman, M.; Talib, I.A.; Farma, R.; Omar, R.; Ishak, M.M.; Basri, N.H.; Dolah, B.N.M. Effect of Compression Pressure on the Physical and Electrochemical Properties of Activated Carbon Monolith Electrodes for Supercapacitor Application. *Adv. Mater. Research* **2012**, 501, 13-18.

(27) Liu, M.-C.; Kong, L.-B.; Zhang, P.; Luo, Y.-C.; Kang, L. Porous Wood Carbon Monolith for High Performace Supercapacitors. *Electrochim. Acta* **2012**, 60, 443-448.

(28) Calvo, E.G.; Ferrera-Lorenzo, N.; Menendez, J.A.; Arenillas, A. Microwave Synthesis of Micro-Mesoporous Carbon Xerogels for High Performance Supercapacitors. *Micropor. Mesopor. Mater.* **2013**, 168, 206-212.

(29) Zeller, M.; Lorrmann, V.; Reichenauer, G.; Wiener, M.; Pflaum, J. Relationship between Structural Properties and Electrochemical Characteristics of Monolithic Carbon Xerogel-Based Electrochemical Double-Layer Electrodes in Aqueous and Organic Electrolytes. *Adv. Energy Mater.* **2012**, 2, 598-605.

(30) Yeon, S-H; Knoke, I.; Gogotsi, Y.; Fischer, J. E. Enhanced Volumetric Hydrogen and Methane Storage Capacity of Monolithic Carbide-Derived Carbon. *Microp. Mesop. Mater.* **2010**, 131, 423-428.

(31) Sevilla, M.; Fuertes, A.B. Fabrication of Porous Carbon Monoliths with a Graphitic Framework. *Carbon* **2013**, 56, 155-166.

(32) Goodman, P.A.; Li, H.; Gao, Y.; Lu, Y.F.; Stenger-Smith, J.D.; Redepenning, J. Preparation and Characterization of High Surface Area, High Porosity Carbon Monoliths from Pyrolyzed Bovine Bone and their Performance as Supercapacitor Electrodes. *Carbon* **2013**, 55, 291-298.

(33) Kunowsky, M.; Garcia-Gomez, A.; Barranco, V.; Rojo, J.M.; Ibañez, J.; Carruthers, J.D.; Linares-Solano, A. Dense Carbon Monoliths for Supercapacitors with Outstanding Volumetric Capacitances. *Carbon* **2014**, 68, 553-562.

(34) Stoeckli, F. in: Patrick, J. (Ed), Porosity in Carbons Characterization and Applications, Arnold, London; 1995 (Chapter 3).

(35) Stoeckli, F.; Centeno, T.A. Optimization of the Characterization of Porous Carbons for Supercapacitors. *J. Mater. Chem. A* **2013**, 1, 6865-6873

(36) Centeno, T.A.; Stoeckli, F. The Assessment of Surface Areas in Porous Carbons by Two Model-Independent Techniques, the DR Equation and DFT. *Carbon* **2010**, 48, 2478-2486.

(37) Tian, Y.; Yan, J.-W., Xue, R.; Yi, B.L. Influence of Electrolyte Concentration and Temperature on the Capacitance of Activated Carbon. *Acta Phys.-Chim. Sin.* **2011**, 27(2), 479-485.

(38) Andreas, H.A.; Conway, B. Examination of the Double-Layer Capacitance of an High Specific-Area C-Cloth Electrode as Titrated From Acidic to Alkaline pHs. *Electrochim. Acta* **2006**, 51, 6510-6520.

(39) Raymundo-Piñero, E.; Kierzek, K.; Machnikowski, J.; Beguin, F. Relationship between the Nanoporous Texture of Activated Carbons and Their Capacitance Properties in Different Electrolytes. *Carbon* **2006**, 44, 2498-2507.

(40) Lee, H.Y.; Goodenough, J.B. Supercapacitor Behavior with KCl Electrolyte. *J. Solid State Chem.* **1999**, 144, 220-223.

(41) Pang, S.C.; Anderson, M.A.; Chapman, T.W. Novel Electrode Materials for Thin-Film Ultracapacitors: Comparison of Electrochemical Properties of Sol-Gel Derived and Electrodeposited Manganese Dioxide. *J. Electrochem. Soc.* **2000**, 147(2), 444-450.

(42) Nian, Y.R.; Teng, H. Nitric Acid Modification of Activated Carbon Electrodes for Improvement of Electrochemical Capacitance. *J. Electrochem. Soc.* **2002**, 149(8), A1008-A1014.

(43) Bleda-Martinez, M.J.; Macia-Agullo, J.A.; Lozano-Castello, D.; Morallon, E.; Cazorla-Amoros, D.; Linares-Solano, A. Role of Surface Chemistry on Electric Double Layer Capacitance of Carbon Materials. *Carbon* **2005**, 43, 2677-2684.

(44) Okajima, K.; Ohta, K.; Sudoh, M. Capacitance Behavior of Activated Carbon Fibers with Oxygen-Plasma Treatment. *Electrochim. Acta* **2005**, 50 2227-2231.

(45) Wu, F.-C.; Tseng, R.-L.; Hu, C.-C.; Wang, C.-C. Effects of Pore Structure and Electrolyte on the Capacitive Characteristics of Steam- and KOH-Activated Carbons for Supercapacitors. *J. Power Sources* **2005**, 144, 302-309.

(46) Carbons for Electrochemical Energy Storage and Conversion Systems. Ed. F. Beguin and E. Frackowiak. Chapter 5. CRC Press, Taylor and Francis Group. ISBN: 978-1-4200-5307-4. 2010

(47) Centeno, T.A.; Hahn, M.; Fernandez, J.A.; Kotz, R.; Stoeckli, F. Correlation between Capacitances of Porous Carbons in Acidic and Aprotic EDLC Electrolytes. *Electrochem. Commun.* **2007**, 9, 1242-1246.

(48) Bao, Q.; Bao, S.; Li, C.M.; Qi, X.; Pan, C.; Zhang, J.; Lu, Z.; Li, Y.; Tang, D.Y.; Zhang, S.; Lian, K . Supercapacitance of Solid Carbon Nanofibers Made from Ethanol Flames. *J. Phys. Chem. C* **2008**, 112, 3612-3618.

(49) Barranco, V.; Lillo-Rodenas, M.A.; Linares-Solano, A.; Oya, A.; Pico, F.; Ibañez, J.; Agullo-Rueda, F.; Amarilla, J.M.; Rojo, J.M. Amorphous Carbon Nanofibers and Their Activated Carbon Nanofibers as Supercapacitor Electrodes. *J. Phys. Chem. C* **2010**, 114 10302-10307.

(50) Eliad, L.; Salitra, G.; Soffer, A.; Aurbach, D. Ion Sieving Effects in the Electrical Double Layer of Porous Carbon Electrodes: Estimating Effective Ion Size in Electrolytic Solutions. *J. Phys. Chem. B* **2001**, 105, 6880-6887.

(51) Eliad, L.; Pollak, E.; Levy, N.; Salitra, G.; Soffer, A.; Aurbach, D. Assessing Optimal Pore-to-Ion size Relations in the Design of Porous Poly(vinylidene chloride) Carbons for EDL Capacitors. *Appl. Phys. A* **2006**, 82, 607-613.

(52) Meng, S.; Chakarov, O.V.; Kasemo, B.; Gao, S. Two-Dimensional Hydration Shells of Alkali Metal Ions at a Hydrophobic Surface. *J. Chem. Phys.* **2004**, 121, 12572-12576.

(53) An, H.-L.; Liu, Y.-Z.; Zhang, S.-H.; Zhan, Y.; Zhang, H.-L. Properties of Hydrated Alkali Metals Aimed at the Ion Channel Selectivity. *Chin. Phys. Lett.* **2008**, 25(9), 3165-3168.

(54) Imberti, S.; Botti, A.; Bruni, F.;Cappa, G.; Ricci, M.A.; Soper, A.K. Ions in Water: the Microscopic Structure of Concentrated Hydroxide Solutions. *J. Chem. Phys.* **2005**, 122, 194509 (1-9).

(55) Aziz, E.F.; Ottosson, N.; Faubel, M.; Hertel, I.V.; Winter, B. Interaction between Liquid Water and Hydroxide Revealed by Core-Hole De-Excitation. *Nature* **2008**, 455, 89-91.

(56) Feng, G.; Qiao, R.; Huang, J.; Sumper, B.G.; Meunier, V. Ion Distribution in Electrified Micropores and Its Role in the Anomalous Enhancement of Capacitance. *ACS Nano* **2010**, 4, 2382-2390.

TABLE of CONTENTS (TOC)